Available online at www.sciencedirect.com

ScienceDirect

Journal of Computational and Applied Mathematics 218 (2008) 317–328

JOURNAL OF COMPUTATIONAL AND APPLIED MATHEMATICS

www.elsevier.com/locate/cam

On grid generation for numerical models of geophysical fluid dynamics

Ludmila Bourchtein*, Andrei Bourchtein

Institute of Physics and Mathematics, Pelotas State University, Rua Anchieta 4715 bloco K, ap.304, 96015-420 Pelotas, Brazil

Received 28 September 2006; received in revised form 16 January 2007

Abstract

A simple geometric condition that defines the class of classical (stereographic, conic and cylindrical) conformal mappings from a sphere onto a plane is derived. The problem of optimization of computational grid for spherical domains is solved in an entire class of conformal mappings on spherical (geodesic) disk. The characteristics of computational grids of classical mappings are compared for different spherical radii of geodesic disk. For a rectangular computational domain, the optimization problem is solved in the class of classical mappings and respective area of the spherical domain is evaluated.

MSC: 30C20; 65M50; 86A30

Keywords: Geophysical fluid dynamics; Numerical models; Conformal mappings; Computational grids

1. Introduction

Many processes of the geophysical fluid dynamics are of a large scale; consequently we must account for the earth's spherical shape, which implies formulation of related mathematical models in a spherical geometry. Variations of the temperature, pressure and wind, which define the weather phenomena, global atmospheric and ocean circulations are examples of such kind of problems. Due to the complexity of the mathematical models only a few particular solutions are known and, in the general case, approximated solutions can be found by the application of numerical methods. Therefore, their quality depends on principal properties of numerical schemes: accuracy, stability and efficiency.

Generation of the computational grids is an important step for the definition of the scheme properties. In this paper we are mainly concerned with the structured grids for finite-difference schemes, which are used in the majority of the models of geophysical fluid dynamics. Therefore, some of our considerations and conclusions cannot be extended to other frameworks, such as unstructured grids or mesh-free approach, which emerged in the geophysical fluid modeling in the last decade (e.g., [1,15]).

Computational grids based on the spherical coordinates are highly nonuniform, especially in the polar regions, which causes the problems for both dynamical and physical parts of the numerical schemes. In fact, the accuracy of

* Corresponding author. Tel.: +55 53 32285445; fax: +55 53 32757343.
E-mail address: bourchtein@terra.com.br (L. Bourchtein).

0377-0427/$ - see front matter © 2007 Elsevier B.V. All rights reserved.
doi:10.1016/j.cam.2007.02.005

any scheme depends on the largest physical mesh size in the chosen domain and, therefore, the use of nonuniform physical grids leads to the loss of accuracy in the subdomains of the greatest mesh size or unnecessary refinement in the subdomains of the smallest mesh size. Furthermore, absolute majority of the schemes used in the atmosphere and ocean dynamics are explicit or semi-implicit and, therefore, their time steps must be proportional to the space mesh size in order to satisfy the Courant–Friedrichs–Lewy criterion. Hence, excessive refinement of spatial resolution can impose physically unjustified restriction on the allowable time step. Other problems of nonuniform resolution are related to physical parameterizations used in a model. The choice of the parameterization scheme could be problematic because of the different definition of subgrid scales in the regions with different physical mesh sizes. Thus, a smaller difference among physical mesh sizes in the considered domain results in a more efficient numerical scheme with more reliable solutions. Of course, these considerations cannot be applied if nonuniform resolution is a desirable property of the scheme resulting from the simulation goals (for example, when local refinement of solution is needed in some subregions) or from the nature of physical processes (for example, when the space variability of physical parameters is highly nonuniform). In such cases other approaches can be more promising such as unstructured grid generation or mesh-free approach. Some models based on unstructured grids have been recently developed for ocean modeling, showing that an efficient unstructured mesh adaptation strategy may produce meshes with a ratio greater than 50 between the smallest and the greatest elements [4,11], but their discussion is out of scope of our research.

One of the most widespread approaches to grid generation for problems in spherical geometry is a mapping of a spherical domain onto a plane. Usually, these mappings are conformal, which assures three important properties: a more simple form of the primitive hydrodynamic equations, locally isotropic treatment of derivatives and smoothness of physical mesh size variation (due to analyticity of transformation functions). In atmospheric and ocean dynamics, the most used conformal mappings are stereographic, conic and cylindrical, also called the classical projections. The first two projections are usually applied to the regions of high and middle latitudes and the last mapping is commonly used for tropical regions. Different examples of their application can be found in the regional and meso-scale atmospheric models used in operational practice and research (e.g., [2,3,12,14,16,19,22]). All these mappings can be tangent or secant depending on the type of intersection between sphere and the respective projection surface (plane, cone or cylinder). If conformal mappings are based on geographical (polar) latitude–longitude coordinates then they are called polar projections, otherwise, they are called rotated or oblique projections [7,18]. The rotated spherical coordinates can be obtained from the polar ones by moving the pole to the chosen point and the rotated projections are derived from the rotated spherical coordinates in the same way as polar mappings are derived from geographical spherical coordinates.

Even though conformal projections from a sphere onto a plane have been known in different fields of science for centuries, they still give rise to various problems. As far as we know, the problem of the generation of the most uniform grids for spherical domains has not been completely solved neither for the whole class of the conformal mappings nor for the subclasses of the classical mappings.

In this study we consider a geometric characterization of classical mappings and derive analytical solutions for some spherical domains of specific geometry. The text is structured as follows. In Section 2 we show that the classical polar mappings form a class of all conformal projections whose mapping factor does not depend on the longitude. In Section 3, considering the problem for a spherical (geodesic) disk, we employ the Chebyshev–Milnor theory to show that the "best" stereographic mapping is the "best possible" projection in the entire set of conformal mappings and compare the degree of the distortion caused by different projections of a sphere onto a plane. In Section 4 we find the "best" classical mapping for the spherical domain with a rectangular image and evaluate the spherical area corresponding to the "best" mapping. Final remarks are presented in the last section.

2. Geometric characterization

For subsequent references, let us recall some basic definitions of the specific conformal mappings. Using spherical coordinates ξ (radius), λ (longitude) and θ (colatitude) one can write the formulas of the stereographic tangent projection of the sphere $\xi = a$ onto a plane provided with polar coordinates r, φ in the form [7,18,22]:

$$\varphi = \lambda, \quad r = 2a \tan\frac{\theta}{2}, \quad \lambda \in [0, 2\pi), \quad \theta \in [0, \pi). \tag{2.1}$$

The set of the conic conformal projections tangent to the sphere at the points of colatitude $\theta_0 \in (0, \pi/2)$ is defined as follows [7,18]:

$$\varphi = n\lambda, \quad r = a\frac{\sin\theta_0}{n}\left(\tan\frac{\theta}{2}\Big/\tan\frac{\theta_0}{2}\right)^n, \quad \lambda \in [0, 2\pi), \quad \theta \in (0, \pi), \tag{2.2}$$

where $n = \cos\theta_0 \in (0, 1)$ is the parameter specifying the mapping of this set. The cylindrical conformal mapping tangent to the sphere at the points of the equator has the form [7,18,22]:

$$x = a\lambda, \quad y = a\ \ln\cot\frac{\theta}{2}, \quad \lambda \in [0, 2\pi), \quad \theta \in (0, \pi), \tag{2.3}$$

where x, y are Cartesian coordinates of the projection plane.

The important characteristic of a conformal mapping is its mapping factor (scale function) m defined as the ratio between the elementary arc lengths along a planar curve and respective spherical curve. For the above mappings the respective mapping factors can be expressed as follows [7,18,22]:

$$m_{\mathrm{str}} = \frac{2}{1+\cos\theta}, \tag{2.4}$$

$$m_{\mathrm{con}} = \frac{\sin\theta_0}{\sin\theta}\left(\tan\frac{\theta}{2}\Big/\tan\frac{\theta_0}{2}\right)^n \tag{2.5}$$

and

$$m_{\mathrm{cyl}} = \frac{1}{\sin\theta}. \tag{2.6}$$

To evaluate the degree of distortion caused by a projection of the sphere surface onto a plane, we use the following variation coefficient:

$$\alpha = \frac{m_{\max}}{m_{\min}}, \tag{2.7}$$

which is one of the standard measures of distortion in cartography [13,17]. In Section 3 we derive this coefficient as a natural measure of efficiency of computational grids for numerical schemes. Two projections are considered equivalent on chosen domain if they produce the same variation coefficient.

To deduce a geometric property of the class of classical (i.e., stereographic, conic and cylindrical) conformal mappings, we consider any conformal mapping as a composition of two conformal transformations: the first is the stereographic projection of a primitive spherical domain onto an auxiliary planar domain and the second maps the last domain onto a specific final domain.

Before application of the second mapping it is suitable to cut the complex stereographic w-plane ($w = u + \mathrm{i}v = \rho\mathrm{e}^{\mathrm{i}\psi}$) along the positive real axis. It corresponds to the cut of the primitive sphere along the meridian $\lambda = 2\pi$ (or $\lambda = 0$) and makes possible application of all mappings to be considered in this section on the auxiliary domain

$$D = \{w = \rho\mathrm{e}^{\mathrm{i}\psi},\ 0 < \psi < 2\pi\}.$$

The second conformal mapping

$$z = x + \mathrm{i}y = f(w)$$

transforms the domain D onto $E = f(D)$. Obtained composition of two mappings is the conformal transformation which maps the chosen domain on the sphere onto the domain E. The mapping factor of this composition is

$$m = \frac{2}{1+\cos\theta}|f'(w)|. \tag{2.8}$$

Hereinafter we use standard notations for the first $f'(w)$ and second $f''(w)$ derivatives of a complex function $f(w)$.

Obviously, the tangent stereographic projection (2.1) is generated by the function

$$z = f(w) = w.$$

Let us note that the functions

$$f(w) = Aw + B, \quad A, B \in C \ \ (A \neq 0) \tag{2.9}$$

do not change the values of the variation coefficient (2.7), and therefore all these functions belong to the same equivalence class.

The conic mappings can be generated by the functions

$$z = f_n(w) = w^n, \quad 0 < n < 1, \tag{2.10}$$

which establish a one-to-one correspondence between the domain D and the infinite sector with central angle $2n\pi$. Using polar coordinates in z-plane $z = x + \mathrm{i}y = r\mathrm{e}^{\mathrm{i}\varphi}$, the respective composite transformations and the final domains can be written as follows:

$$\varphi = n\lambda, \quad r = \rho^n = (2a)^n \left(\tan\frac{\theta}{2}\right)^n, \tag{2.11}$$

$$E = \{z = r\mathrm{e}^{\mathrm{i}\varphi}, \ 0 < \varphi < 2n\pi\}.$$

Each function f_n with specific value of n generate their own equivalence class, which contains also all the functions

$$f(w) = Aw^n + B, \quad A, B \in C \ \ (A \neq 0). \tag{2.12}$$

If

$$A = \frac{a}{n \cdot (2a)^n} \tan\theta_0 \cdot \left(\tan\frac{\theta_0}{2}\right)^{-n}, \quad B = 0,$$

then (2.11) represents the conformal conic mappings (2.2).

Finally, using the function

$$z = f(w) = -\mathrm{i}a \ln\frac{w}{2a}, \tag{2.13}$$

which maps the domain D onto the infinite vertical strip

$$E = \{z = x + \mathrm{i}y, \ 0 < x < 2a\pi\},$$

we obtain the cylindrical mapping (2.3). This mapping generates one more equivalence class including all the functions

$$f(w) = A \ln w + B, \quad A, B \in C \ \ (A \neq 0). \tag{2.14}$$

Now let us consider conformal mappings whose scale factor (2.8) does not depend on the longitude λ. Using the derivative in polar coordinates

$$f'(w) = -\frac{\mathrm{i}}{w}\left(\frac{\partial x}{\partial\psi} + \mathrm{i}\frac{\partial y}{\partial\psi}\right), \tag{2.15}$$

the above condition gives

$$\frac{\partial|f'(w)|}{\partial\lambda} = \frac{1}{\rho}\frac{\partial\sqrt{(\partial x/\partial\psi)^2 + (\partial y/\partial\psi)^2}}{\partial\psi} = \frac{1}{\rho \cdot |f'(w)|}\left(\frac{\partial x}{\partial\psi}\frac{\partial^2 x}{\partial\psi^2} + \frac{\partial y}{\partial\psi}\frac{\partial^2 y}{\partial\psi^2}\right) = 0. \tag{2.16}$$

Since $f(w)$ is a conformal mapping, $f'(w) \neq 0, \ \forall w \in D$. The second derivative of $f(w)$ has the following form in polar coordinates:

$$f''(w) = -\frac{1}{w^2}\left(\frac{\partial^2 x}{\partial\psi^2} + \mathrm{i}\frac{\partial^2 y}{\partial\psi^2}\right) - \frac{1}{w}f'(w),$$

that is,

$$\frac{\partial^2 x}{\partial \psi^2} + \mathrm{i}\frac{\partial^2 y}{\partial \psi^2} = -w^2 f''(w) - w f'(w). \tag{2.17}$$

Besides, (2.15) implies

$$\frac{\partial x}{\partial \psi} + \mathrm{i}\frac{\partial y}{\partial \psi} = \mathrm{i} w f'(w). \tag{2.18}$$

Using (2.17) and (2.18), one can rewrite condition (2.16) as follows:

$$\frac{\partial x}{\partial \psi}\frac{\partial^2 x}{\partial \psi^2} + \frac{\partial y}{\partial \psi}\frac{\partial^2 y}{\partial \psi^2} = Re\{(-w^2 f''(w) - w f'(w))(\overline{\mathrm{i} w f'(w)})\} = |w|^2 |f'(w)|^2 \,\mathrm{Re}\left\{\mathrm{i} w \frac{f''(w)}{f'(w)}\right\} = 0. \tag{2.19}$$

Since $f(w)$ is a regular function and $f'(w) \neq 0,\ \forall w \in D$, the function

$$F(w) = \mathrm{i} w \frac{f''(w)}{f'(w)} = g(w) + \mathrm{i} h(w)$$

is regular too. Therefore the Cauchy–Riemann conditions hold

$$\frac{\partial g}{\partial u} = \frac{\partial h}{\partial v}, \quad \frac{\partial g}{\partial v} = -\frac{\partial h}{\partial u}.$$

Eq. (2.19) means that $g(w) = 0$ and, consequently, $\partial h/\partial u = 0,\ \partial h/\partial v = 0$, that is, $h(w) = n,\ n = \mathrm{const} \in R$, or, in terms of the function f,

$$w \frac{f''(w)}{f'(w)} = n. \tag{2.20}$$

If $n = 0$, then it follows from (2.20) that $f''(w) = 0$, that is, one obtains functions (2.9)

$$f(w) = Aw + B, \quad A, B \in C \ \ (A \neq 0).$$

If $n \neq 0$, then (2.20) implies that

$$f'(w) = A w^n, \quad A \in C \ \ (A \neq 0). \tag{2.21}$$

The last equation generates two sets of functions. In the case $n = -1$ one obtains functions (2.14) of cylindrical mappings

$$f(w) = A \ln w + B, \quad A, B \in C \ \ (A \neq 0). \tag{2.22}$$

Otherwise, Eq. (2.21) results in

$$f(z) = \frac{A}{n+1} w^{n+1} + B = A_1 w^{n+1} + B, \quad A_1, B \in C \ \ (A_1 \neq 0), \tag{2.23}$$

that is, conic mappings are generated.

Remark 1. Let us note that functions (2.23) correspond to conic mappings (2.12) if $0 < n + 1 < 1$; in the case $-1 < n + 1 < 0$, these functions represent conic mappings located above the South Pole, which are symmetric to the mappings of the first group with respect to the equator; otherwise ($|n + 1| > 1$) transformations (2.23) are not one-to-one on the entire domain D. However, if one considers only a part of the domain D, for example, a sector with vertex at the origin and opening $2k\pi$, $0 < k < 1$, then functions (2.23) will represent conformal mappings for some values of $|n + 1| > 1$, namely, for $1 < |n + 1| < 1/k$.

Thus, all projections with the mapping factor independent from the longitude consist of stereographic (2.9), conic (2.12) and cylindrical (2.14) projections. Of course, the same is true for oblique projections except for the independence of their mapping factor from a new "non geographical" longitude.

3. Minimization problem for spherical disk

To formulate the minimization problem, we first introduce a quantitative measure for evaluation of the efficiency of the computational grid. Let us consider a fixed spherical domain and different computational grids based on the conformal mapping of this domain onto a plane. If the desired spatial mesh size is h_0, then the ideal grid is uniform with respect to physical mesh size h_0. A real grid is uniform in computational coordinates with a computational mesh size h_1. First, let us consider the choice of the computational mesh size with respect to the desired physical accuracy. Actual (physical) approximation is better (that is, the physical mesh sizes are smaller) in such regions of the computational grid where the mapping factor m has the maximum values ($m_{\max}$) and actual discretization is worse in the regions with the minimum mapping factor ($m_{\min}$). Assuming that general accuracy of numerical scheme is defined by regions with the greatest physical mesh size, the computational mesh size should be chosen in such a way that $h_1 \approx h_0 \cdot m_{\min}$ to assure an approximation equivalent to that with physical mesh size h_0.

Another important characteristic of the numerical scheme, which influences on the choice of the computational mesh size, is its stability. To understand better a situation one can specify the primitive equations in the form of the shallow water system, which is the characteristic model for atmosphere and ocean dynamics. The totality of actual numerical models have a certain degree of explicitness, which usually implies some stability constraint on time step size. In fact, the time step of the majority of the used schemes is subject to numerical stability restriction (called Courant–Friedrichs–Lewy condition) that can be approximately expressed in the form

$$\tau_{\max} \approx \frac{h_1}{m_{\max} \cdot s} = \frac{m_{\min}}{m_{\max}} \cdot \frac{h_0}{s} = \frac{1}{\alpha} \cdot \frac{h_0}{s}, \tag{3.1}$$

where s is the maximum velocity of the physical processes approximated in an explicit way. For instance, s is equal to velocity of gravity waves for an explicit scheme (such as leap-frog scheme); s is equal to the maximum wind speed (that is, the maximum advective speed) if one uses a semi-implicit scheme (for example, Robert's scheme); finally, s represents the modulus of the maximum wind gradient if a semi-Lagrangian semi-implicit method is employed [9,10,20]. Therefore, the number of time steps increases $\alpha = m_{\max}/m_{\min}$ times as compared with an ideal physical grid (with $m \equiv 1$). Consequently, the same scheme considered on the computational grid requires α times more calculations than that on the ideal grid (where $\alpha = 1$). If the form of the primitive equations is of the same level as of the complexity in different coordinates, then the problem of computational grid optimization can be formulated as finding such mapping of the spherical domain that assures the minimum value of the variation coefficient α. This is the case of the shallow water equations (and generally the three-dimensional hydrodynamic equations) because they have a similar structure in the geographical spherical coordinates and in the Cartesian coordinates of arbitrary conformal mapping [21,22].

Besides, in the models of real simulation of atmosphere and ocean dynamics, there are a number of physical blocks for parameterization of subgrid scale processes (vertical convection, turbulence, clouds and condensation, radiation, etc.). If each of these processes is related to a certain space scale (which is a frequent situation in atmospheric dynamics), then computational grids with a greater physical uniformity will assure more uniform definition of subgrid scales over the entire spherical domain, and, consequently, the used parameterizations will be more reliable [9,19].

Therefore, the minimization of the variation coefficient α (2.7) over a given spherical domain Ω is important for efficiency of both dynamical and physical blocks of the numerical hydrodynamic scheme. Obviously, two equivalent conformal mappings generate equivalent grids. The equivalence of such projections has clear physical meaning: one of these projections can be obtained from another one by a change of measure unit for distance.

Now we can solve the minimization problem for spherical disk Ω_γ of the spherical radius $a\gamma$ ($\gamma \in (0, \pi)$) consisting of all sphere points $P = (a, \lambda, \theta)$ whose spherical (geodesic) distance from the centerpoint $P_0 = (a, \lambda_0, \theta_0)$ is less than $a\gamma$: $d_S(P_0, P) \leqslant a\gamma$. By definition, the distance between sphere points P_0 and P is the length of the shortest great circle arc joining these points. Since the spherical disk Ω_γ is symmetric with respect to rotation around its central point, it is natural to expect that the solution of the minimization problem should be found in the class of conformal mappings with the mapping factor independent of the longitude in rotated coordinates.

In what follows we need the following two results, presented, for example in [13,17].

Chebyshev–Milnor Theorem. *If Ω is a simply connected open spherical domain bounded by a twice differentiable curve, then there exists one and, up to a similarity transformation of the plane, only one conformal mapping which*

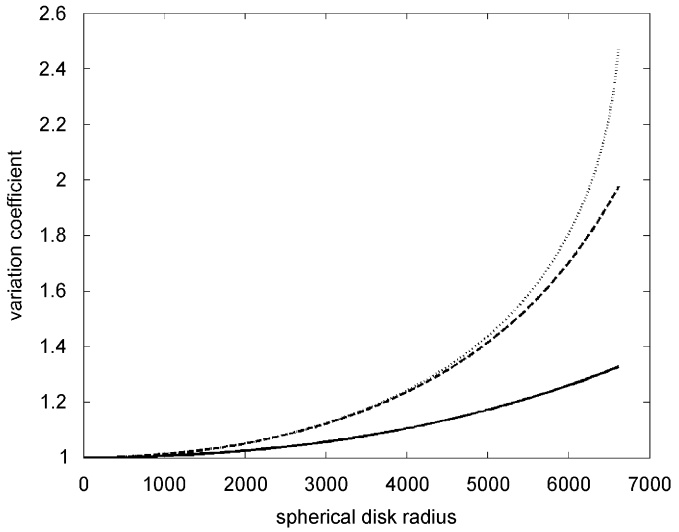

Fig. 1. The variation coefficient plotted as a function of the spherical radius $a\gamma$ given in km. The solid line is for the stereographic mapping, the dashed is for the cylindrical, and the dotted is for conic.

minimizes the variation coefficient (2.7). *The* "*best possible*" *conformal mapping is characterized by the property that its scale function m is constant along the boundary of* Ω.

Chebyshev–Milnor Lemma. *A given positive real-valued function m on* Ω *is the mapping factor associated with some conformal mapping f if, and only if, m is twice differentiable and satisfies the differential equation* $a^2\Delta \ln m = 1$ *in* Ω, *where* Δ *is the Laplace operator*.

A direct application of this theorem shows that the stereographic projection tangent to the spherical disk Ω_γ at the centerpoint P_0 is the "best possible" projection in the entire class of conformal mappings. In fact, since the spherical disk is of required geometry and smoothness, the theorem assures the existence of the "best possible" mapping. With no loss of generality we can consider the centerpoint P_0 be the North Pole (otherwise, it is sufficient to apply the theorem in rotated spherical coordinates). Evidently, the above chosen stereographic mapping has the smooth mapping factor with constant value $m = 2/(1 + \cos\gamma)$ on the disk boundary $\partial\Omega_\gamma$. Therefore, this mapping is the "best possible". Any other "best possible" mapping can be obtained from this one by a similarity transformation, that is, applying conformal mapping (2.9) to the domain obtained after the "best" stereographic mapping.

In Fig. 1, the variation coefficient of the classical conformal mappings is plotted as a function of the spherical radius $a\gamma$. The "best" conic and cylindrical mappings were found using the results in [5]. It can be seen that the "best" stereographic mappings assure visibly better uniformity than two others for spherical radius greater than 4000 km. If the spherical radius is smaller than 2000 km, then the differences between projections can be ignored.

4. Minimization problem for computational rectangle

Since the computational domains are usually rectangular, it is of practical interest to find out what happens if a spherical domain has rectangular image in the plane. Using the Chebyshev–Milnor theorem one can immediately conclude that neither of the classical mappings (stereographic, conic, or cylindrical) minimizes the variation coefficient in the class of conformal mappings if a domain Ω is different from the spherical disk. Nevertheless, it is natural to expect that the "best" classical mapping should be close to the "best" conformal one because the nonuniformity of spherical coordinates is the consequence of the change of the physical mesh size along the latitude when one is moving in the equator-pole direction. If the displacement is in the west-east direction then the mesh size does not change. Moreover, the physical mesh size along the longitude is the same for any location on the sphere. Therefore, it is natural to look for solutions of the problem of uniform grid generation within the set of mappings that do not change the physical mesh size along the longitude, that is, the mappings with the scale factor independent from the longitude.

In [5,6] it was shown that the variation coefficients of the "best" stereographic, cylindrical and conic mappings satisfy the following inequality:

$$\alpha_{\text{str}} < \alpha_{\text{cyl}} < \alpha_{\text{con}}.$$

Therefore, it is sufficient to minimize the variation coefficient in the class of stereographic mappings in order to find the "best" projection among the classical ones.

In this section we consider the problem of optimization of computational rectangular domain with respect to the choice of its location. Naturally, we associate the centerpoint of computational grid with the centerpoint of the respective spherical domain. This problem has two equivalent interpretations: first, one should find the "best" oblique projection for a fixed location of the computational grid centered regarding the origin of Cartesian coordinates; second, one should find the "best" location of computational grid for specific stereographic mapping, for example, for the polar one. The last approach is used in the following considerations. It should be note that the original spherical domain corresponding to the computational rectangle has a rather complex geometry in spherical coordinates and its area ("true" area) depends on the location of the computational domain. Evidently, the mapping with the minimal α could be not optimal one if the respective "true" area is smaller than that for other mappings. Therefore, to optimize the computational grid we should parallely consider the problem of minimization of the variation coefficient and maximization of the "true" area.

In order to restrict a set of mappings to be considered, we note that any secant stereographic projection has an equivalent tangent projection located on a plane parallel to the secant one. Therefore, it is sufficient to study only the tangent projections. Let us consider the polar stereographic projection provided with the Cartesian coordinates (x, y) whose origin coincides with the North Pole. Location of computational domain in the form of a rectangle R with sides of the fixed length $2b$ and $2c$ can be defined by the only parameter if we make an assumption that the rectangle sides are parallel to coordinate axis (this is quite a natural assumption because of the invariance of the properties of the stereographic mapping regarding rotation about the pole axis). The abscissa s of the points of the left side can be chosen as such a parameter (see Fig. 2). Due to symmetry with respect to the axis oy we can only consider the values $s \geqslant -b$.

First we evaluate the spherical area ("true" area) corresponding to the chosen rectangle. The standard formula for calculation of area of a surface defined parametrically has the form [8]:

$$A = \int_R\int \sqrt{EG - F^2}\,\mathrm{d}x\,\mathrm{d}y, \tag{4.1}$$

where

$$E = \left(\frac{\partial X}{\partial x}\right)^2 + \left(\frac{\partial Y}{\partial x}\right)^2 + \left(\frac{\partial Z}{\partial x}\right)^2, \quad G = \left(\frac{\partial X}{\partial y}\right)^2 + \left(\frac{\partial Y}{\partial y}\right)^2 + \left(\frac{\partial Z}{\partial y}\right)^2,$$
$$F = \frac{\partial X}{\partial x}\frac{\partial X}{\partial y} + \frac{\partial Y}{\partial x}\frac{\partial Y}{\partial y} + \frac{\partial Z}{\partial x}\frac{\partial Z}{\partial y} \tag{4.2}$$

and X, Y, Z are the Cartesian space coordinates.

Using the formulas (2.1) of stereographic mapping together with the polar coordinate relations

$$x = r\,\cos\,\varphi, \quad y = r\,\sin\,\varphi$$

and the sphere equations

$$X = a\sin\theta\cos\lambda, \quad Y = a\sin\theta\sin\lambda, \quad Z = a\cos\theta$$

we can express the coefficients (4.2) in the form

$$E = G = \frac{16a^4}{(4a^2 + x^2 + y^2)^2}, \quad F = 0. \tag{4.3}$$

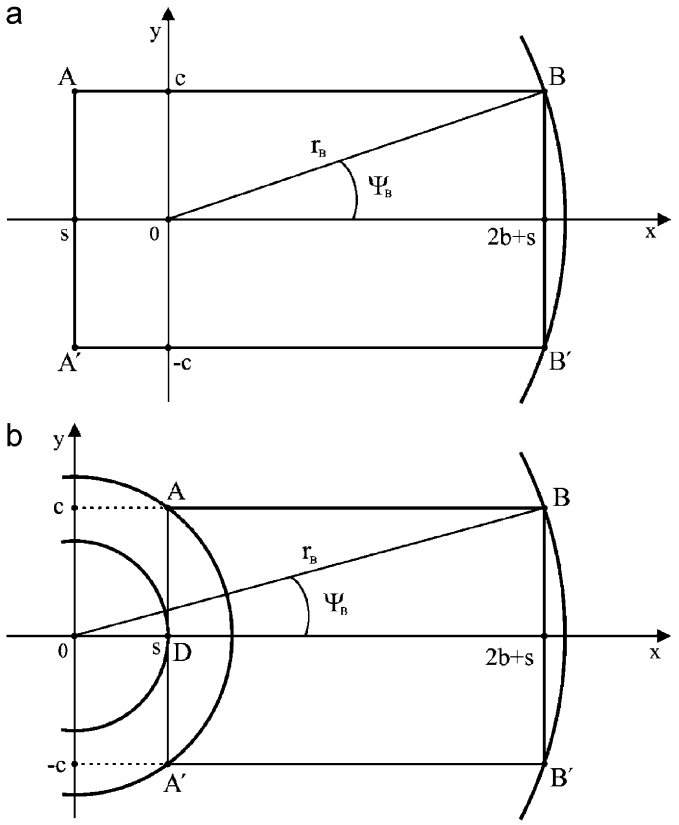

Fig. 2. (a) Rectangle R in stereographic plane, the case $-b \leqslant s \leqslant 0$. (b) Rectangle R in stereographic plane, the case $s > 0$.

Substituting (4.3) in (4.1) and applying some algebra, we obtain

$$\begin{aligned} A &= \int_R\int \frac{16a^4}{(4a^2+x^2+y^2)^2}\,\mathrm{d}x\mathrm{d}y = \int_s^{s+2b} \mathrm{d}x \int_{-c}^{c} \frac{16a^4}{(4a^2+x^2+y^2)^2}\,\mathrm{d}y \\ &= 4a^2 \frac{s+2b}{\sqrt{4a^2+(s+2b)^2}} \arctan \frac{c}{\sqrt{4a^2+(s+2b)^2}} \\ &\quad -4a^2 \frac{s}{\sqrt{4a^2+s^2}} \arctan \frac{c}{\sqrt{4a^2+s^2}} + 4a^2 \frac{c}{\sqrt{4a^2+c^2}} \left[\arctan \frac{s+2b}{\sqrt{4a^2+c^2}} - \arctan \frac{s}{\sqrt{4a^2+c^2}}\right]. \end{aligned} \tag{4.4}$$

The first derivative of function $A(s)$:

$$\begin{aligned} A'(s) &= \frac{16a^4}{(4a^2+(s+2b)^2)^{3/2}} \arctan \frac{c}{\sqrt{4a^2+(s+2b)^2}} - \frac{16a^4}{(4a^2+s^2)^{3/2}} \arctan \frac{c}{\sqrt{4a^2+s^2}} \\ &\quad + \frac{16a^4 c}{(4a^2+(s+2b)^2)(4a^2+c^2+(s+2b)^2)} - \frac{16a^4 c}{(4a^2+s^2)(4a^2+c^2+s^2)} \end{aligned}$$

is negative for any $s > -b$, because the differences between the first two terms and the second pair of the terms are negative in this case. Therefore, function $A(s)$ is strictly decreasing on the whole interval $s \in [-b, +\infty)$, that is, the maximum true area are covered when domain R is centered at the pole point and it is defined by the formula:

$$A_{\max} = \frac{8a^2 b}{\sqrt{4a^2+b^2}} \arctan \frac{c}{\sqrt{4a^2+b^2}} + \frac{8a^2 c}{\sqrt{4a^2+c^2}} \arctan \frac{b}{\sqrt{4a^2+c^2}}. \tag{4.5}$$

If we rewrite (4.4) in the form

$$A = 4a^2 \frac{s+2b}{\sqrt{4a^2+(s+2b)^2}} \arctan \frac{c}{\sqrt{4a^2+(s+2b)^2}} - 4a^2 \frac{s}{\sqrt{4a^2+s^2}} \arctan \frac{c}{\sqrt{4a^2+s^2}} + 4a^2 \frac{c}{\sqrt{4a^2+c^2}} \arctan \frac{2b\sqrt{4a^2+c^2}}{4a^2+c^2+s(s+2b)}, \tag{4.6}$$

then it becomes clear that the "true" area tends to 0 as s approaches infinite, that is, the area vanishes as the centerpoint approaches the South Pole.

Now we evaluate the variation parameter (2.7):

$$\alpha = \frac{m_{\max}}{m_{\min}}, \quad m = \frac{2}{1+\cos\theta}. \tag{4.7}$$

If the point O (the image of the North Pole) lays within the rectangle R or on its left boundary (that is, $s \in [-b, 0]$), then the mapping factor (4.7) has the minimum value at the point O and the maximum value at the points B and B', which are the images of two spherical points the most distant from the North Pole (see Fig. 2a):

$$m_{\min} = m(O) = m(\theta = 0) = 1, \quad m_{\max} = m(B) = m(B').$$

Since

$$\tan\frac{\theta_B}{2} = \frac{\sqrt{c^2+(2b+s)^2}}{2a} \tag{4.8}$$

(see Fig. 2a), we obtain

$$\alpha(s) = m_{\max} = 1 + \frac{c^2+(2b+s)^2}{4a^2}.$$

Evidently, α is an increasing function on $[-b, 0]$ and, consequently,

$$\alpha_{\min} = \alpha(-b) = 1 + \frac{c^2+b^2}{4a^2}.$$

If the rectangle R does not contain the image point of the North Pole (that is, $s \in (0, +\infty)$), then the point D is the image of the nearest point to the North Pole and the points B and B' are the images of the most distant points (see Fig. 2b):

$$m_{\min} = m(D), \quad m_{\max} = m(B) = m(B').$$

The angle θ_D can be defined by the formula (see Fig. 2b)

$$\tan\frac{\theta_D}{2} = \frac{s}{2a}$$

and θ_B is given by (4.8) as before. Therefore,

$$\alpha(s) = \frac{4a^2+c^2+(2b+s)^2}{4a^2+s^2} = 1 + \frac{c^2+4b^2+4bs}{4a^2+s^2}. \tag{4.9}$$

Since

$$\alpha'(s) = \frac{-4bs^2 - 2s(c^2+4b^2) + 16a^2b}{(4a^2+s^2)^2},$$

function (4.9) is strictly increasing on the interval $(0, s_0)$ and strictly decreasing on the interval $(s_0, +\infty)$, where

$$s_0 = \frac{-(c^2+4b^2) + \sqrt{(c^2+4b^2)^2 + 64a^2b^2}}{4b}.$$

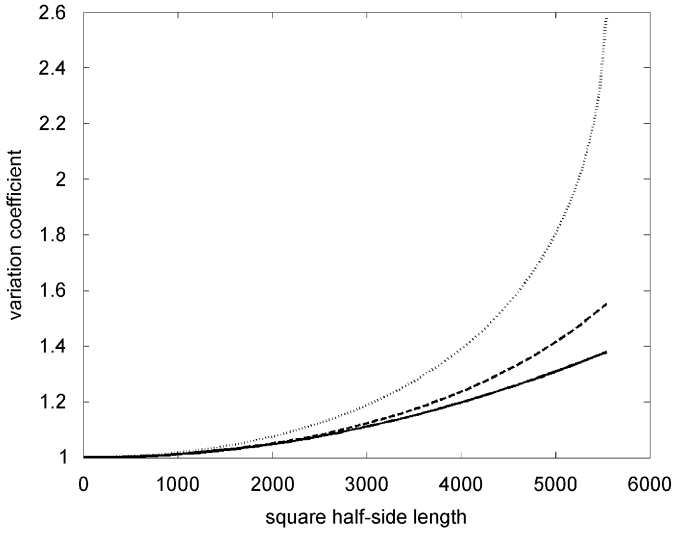

Fig. 3. The variation coefficient plotted as a function of the square half-side length given in km. The solid line is for the stereographic mapping, the dashed is for the cylindrical, and the dotted is for conic.

Using the limit points 0 and $+\infty$ in (4.9), we obtain

$$\alpha(0) = 1 + \frac{c^2 + 4b^2}{4a^2}$$

and

$$\alpha(+\infty) = 1.$$

However, as it was shown above, the last result is referred to the zero area spherical domain. It can be shown that

$$0 < s_0 < 2a - b$$

and

$$\alpha(2a - b) > \alpha(0).$$

That is, the point $s = 0$ is the global minimum point of function (4.9) over the whole interval $[0, 2a - b]$. On the other hand, it can be shown that the "true" area of the rectangle R at the point $s = 2a - b$ is more than two times smaller than the maximum area (4.5). Note that the point $s = 2a - b$ defines the rectangle R with the centerpoint corresponding to the spherical point at the equator. Therefore, there is no sense to use the centerpoints from the South Hemisphere because the "true" area function decreases much faster than the alpha function.

Thus, the most uniform grid is that centered at the North Pole. Besides, this grid covers the maximum spherical area. Consequently, if the centerpoint of the spherical domain does not coincide with the North Pole, then the most uniform stereographic grid is obtained by using oblique mapping with the pole located at the given centerpoint and the rectangle R centered at that point in the same way as in the polar coordinates. Numerical evaluations of the variation coefficient for classical mappings on the computational square are presented in Fig. 3. One can see that the curves are similar to those shown in Fig. 1, except that the variation coefficients of the cylindrical and stereographic mappings in Fig. 3 are much closer than in the case of the spherical disk. It is because a square in the cylindrical projection reproduces a square in spherical coordinates, while stereographic and conic squares represent images of the spherical domains with curvilinear boundaries.

5. Conclusions

In this study we have considered the problem of the generation of computational grids for limited area geophysical fluid models. The following results have been demonstrated: a conformal projection of sphere surface is classical if, and only if, its mapping factor is independent from the longitude; among all the conformal mappings of the spherical disk, the stereographic projection tangent to the spherical disk at its center assures the minimum possible distortion; among the classical projections, the most uniform computational rectangular domain is obtained by the stereographic projection tangent to the sphere at the domain center.

The obtained results can be used for the construction of more uniform structured grids for regional and mesoscale models of the atmosphere and ocean. The application is straight forward for any model already designed in conformal coordinates: the only changes to be made consist of the recalculation of the mapping factor according to the formulas of the best stereographic projection and the appropriate definition of the initial fields (pressure, temperature, velocity components, etc.) and the required model parameters (Coriolis parameter, topography, etc.) at the stereographic grid points. All these modifications should be made only once, before the start of the main loop of the scheme. All computations during the scheme execution remain the same, except that the time step can be increased due to the advantage of the best stereographic mapping over other conformal mappings.

Acknowledgments

We are grateful to two anonymous reviewers for their valuable comments on the original version of the manuscript. This research was supported by the Brazilian science foundation CNPq.

References

[1] W. Bangerth, R. Rannacher, Adaptive Finite Element Methods for Differential Equations, Birkhauser, Basel, 2003.
[2] R. Benoit, M. Desgagne, P. Pellerin, S. Pellerin, Y. Chartier, S. Desjardins, The Canadian MC2: a semi-Lagrangian, semi-implicit wideband atmospheric model suited for finescale process studies and simulation, Monthly Weather Rev. 125 (1997) 2382–2415.
[3] M. Bentsen, G. Evensen, H. Drange, A.D. Jenkins, Coordinate transformation on a sphere using conformal mapping, Monthly Weather Rev. 127 (1999) 2733–2740.
[4] P.-E. Bernard, N. Chevaugeon, V. Legat, E. Deleersnijder, J.-F. Remacle, High-order h-adaptive discontinuous Galerkin methods for ocean modeling, Ocean Dynamics, in press, doi:10.1007/s10236-006-0093-y.
[5] A. Bourchtein, L. Bourchtein, Comparative analysis of conformal mappings used in limited area models of numerical weather prediction, Monthly Weather Rev. 131 (2003) 1759–1768.
[6] L. Bourchtein, A. Bourchtein, One inequality for conformal mappings of spherical domains, Math. Inequality Appl. 9 (2006) 233–246.
[7] L.M. Bugayevskiy, J.P. Snyder, Map Projections. A Reference Manual, Taylor and Francis, London, 1995.
[8] R. Courant, Differential and Integral Calculus, vol. 2, Wiley, New York, 1988.
[9] D.R. Durran, Numerical Methods for Wave Equations in Geophysical Fluid Dynamics, Springer, New York, 1999.
[10] C.A.J. Fletcher, Computational Techniques for Fluid Dynamics, vol. 2, Springer, New York, 1988.
[11] R. Ford, C.C. Pain, M.D. Piggott, A.J.H. Goddard, C.R.E. Oliveira, A.P. Umpleby, A nonhydrostatic finite-element model for three-dimensional stratified oceanic flows. Part I: model formulation, Monthly Weather Rev. 132 (2004) 2816–2831.
[12] H.R. Glahn, Characteristics of map projections and implications for AWIPS-90. TDL Office Note 88–5, National Weather Service, NOAA, 1988.
[13] V.L. Goncharov, The theory of best approximation of functions, J. Approx. Theory 106 (2000) 2–57.
[14] G.A. Grell, J. Dudhia, D.R. Stauffer, A description of the fifth generation Penn State/NCAR mesoscale model (MM5). NCAR Technical Note NCAR/TN-398 + STR, 1994.
[15] G.R. Liu, Mesh Free Methods. Moving Beyond the Finite Element Method, CRC Press, Boca Raton, 2003.
[16] A.E. MacDonald, J.L. Lee, S. Sun, QNH: design and test of a quasi-nonhydrostatic model for mesoscale weather prediction, Monthly Weather Rev. 128 (2000) 1016–1036.
[17] J. Milnor, A problem in cartography, Amer. Math. Monthly 76 (1969) 1101–1112.
[18] F. Pearson, Map Projections: Theory and Applications, CRC Press, Boca Raton, 1990.
[19] A. Staniforth, Regional modeling: a theoretical discussion, Meteorology Atmospheric Phys. 63 (1997) 15–29.
[20] A. Staniforth, J. Côté, Semi-Lagrangian integration schemes for atmospheric models—a review, Monthly Weather Rev. 119 (1991) 2206–2223.
[21] T. Weiyan, Shallow Water Hydrodynamics, Elsevier, Amsterdam, 1992.
[22] D.L. Williamson, Difference approximations for numerical weather prediction over a sphere, GARP Publication Series, No.17, vol. 2, WMO-ICSU, 1979.